Deformation and Fluid Flow in the Huab Basin and Etendeka Plateau, NW Namibia

Eric Salomon [a,*], Daniel Koehn [b], Cees Passchier [a], Peter Chung [b], Tobias Häger [a], Aron Salvona [b], Jennifer Davis [b]

[a]*Institut für Geowissenschaften, Johannes Gutenberg-Universität Mainz, Johann-Joachim-Becher Weg 21, 55128 Mainz, Germany; salomon@uni-mainz.de, cpasschi@uni-mainz.de, tobias.haeger@uni-mainz.de*

[b]*School of Geographical and Earth Sciences, University of Glasgow, Glasgow, G12 8QQ, United Kingdom; daniel.koehn@glasgow.ac.uk, peter.chung@glasgow.ac.uk, aronsalvona@googlemail.com, jennifer.davis@gmail*

*Corresponding author: Eric Salomon, Institut für Geowissenschaften, Johannes Gutenberg-Universität Mainz, Johann-Joachim-Becher Weg 21, 55128 Mainz, Germany, salomon@uni-mainz.de, +49 (0)6131 3920293

Abstract

The Lower Cretaceous Twyfelfontein sandstone formation in the Huab Basin in NW Namibia shows the effects of volcanic activity on a potential reservoir rock. The formation was covered by the Paraná-Etendeka Large Igneous Province shortly before or during the onset of South-Atlantic rifting. Deformation bands found in the sandstone trend mostly parallel to the continental passive margin and must have formed during the extrusion of the overlying volcanic rocks, indicating that their formation is related to South-Atlantic rifting. 2D-image porosity analysis of deformation bands reveals significant porosity reduction from host rock to band of up to 70 %. Cementation of the sandstone, linked to advective hydrothermal flow during volcanic activity, contributes an equal amount to porosity reduction from host rock to band when compared to initial grain crushing. Veins within the basaltic cover provide evidence for hot fluid percolation, indicated by spallation of wall rock and colloform quartz growth, and for a later low-temperature fluid circulation at low pressures indicated by stilbite growth sealing cavities. Sandstone samples and veins in the overlying volcanic rocks show that diagenesis of the Twyfelfontein sandstone is linked to Atlantic rifting and was affected by both hydrothermal and low-thermal fluid circulation.

Keywords

Deformation Bands, cataclastic bands, syn-volcanic faulting, quartz veins, porosity analysis, South Atlantic rifting

1. Introduction

Porous rocks such as sandstones generally serve as reservoirs for hydrocarbons or as aquifers for geothermal or drinking water. A study of the diagenesis, structural change and fluid flow properties of such rocks is of major importance for estimating their reservoir potential (Department of Energy, 2007; Baud et al., 2012). In general, passive continental margins have a high potential for hydrocarbon exploration and margins that are dominated by volcanic activity show that igneous bodies can serve as fluid traps (e.g., Lee et al., 2006; Wu et al., 2006; Gallagher and Dromgoole, 2007; Rohrman, 2007, 2013; Christie and White, 2008; Cukur et al., 2010). Magmatic activity can lead to a significant alteration of sedimentary reservoir rocks by

changing pressure and temperature conditions. For example extrusion of lavas on top of the sediments leads to gravitational loading-induced compaction and an increase in temperature can change fluid composition and speed up diagenetic processes. Examples of sedimentary basins affected by elevated temperatures and subsequent hot fluid flow in response to magmatism are known for example from the NW UK Atlantic margin (Nadin et al., 1997; Wycherley et al., 2003; Baron et al., 2008), the Paraná Basin in southern Brazil (de Ros, 1998), the Solimões Basin in NW Brazil (Lima and de Ros, 2002), the Southern Carnavon basin along the western Australian margin (Baker et al., 2000), the Neuquen Basin in Argentina (Rodriguez Monreal et al., 2009) and rift basins of eastern China (Jin et al., 1999). In order to predict hydrocarbon potential it is therefore important to understand how magmatic activity affects potential reservoir rocks, and how permeability changes during loading, temperature increase and fluid fluxes.

The degree of cementation and the formation of deformation bands can have a significant impact on reservoir quality. Because both processes are known to reduce the porosity they have been studied in detail (Worden and Morad, 2000, and references therein; Fossen et al., 2007, and references therein). Deformation bands are mm-wide zones that accommodate less than a few decimeters of offset (Aydin, 1978). The movement in these zones usually results in grain crushing or sliding and the bands are therefore subdivided into cataclastic (crushing) or disaggregation (sliding) bands (e.g., Antonellini et al., 1994; Fossen et al., 2007). While disaggregation bands typically form at shallow burial levels under low confining pressure and in poorly sorted sandstones (e.g., Antonellini et al., 1994; Kristensen et al., 2013), cataclastic bands form at depths of up to 3 km, commonly in well sorted sandstones (e.g., Zhang et al., 1990; Cashman and Cashman, 2000; Rawling and Goodwin, 2003; Fossen et al., 2007). Exceptions are cataclastic bands that have been reported from unsorted sandstone at shallow burial depth in Corsica, France (Torabi, 2014) and in Provence, France (Ballas et al., 2012). Deformation bands may form in response to faulting of underlying basement rock (Underhill and Woodcock, 1987), either within a damage zone as a precursor of discrete faulting (Shipton and Cowie, 2001), or during throw of an existing fault (Shipton and Cowie, 2003).

Here, we analyze the effects which volcanic activity had on the diagenesis of an aeolian sandstone exposed in the Huab Basin in NW Namibia (**Fig. 1**). The sandstone of the Lower Cretaceous Twyfelfontein Formation (Stanistreet and Stollhofen, 1999) is overlain by volcanic rocks of the ~133-Ma-old Paraná-Etendeka Large Igneous Province (Renne et al., 1992) and a large number of dykes cut through the sandstone. The sandstone was solely overlain and thus buried by the extrusives (Miller, 2008). This geologic setting and the excellent outcrop conditions in Namibia allow detailed analysis of the diagenetic effects and fluid system evolution of a reservoir rock that is affected by igneous activity. Dickinson and Milliken (1995) conducted a first microstructural study of the Twyfelfontein sandstone reporting pressure solution at quartz grain contacts, fracturing of single quartz grains and cementation of these fractures.

The aim of this paper is to characterize deformation, cementation and porosity of Twyfelfontein sandstone and the overlying Etendeka volcanic rocks and to reconstruct details of fluid flow within these rocks in order to give a model for their diagenetic evolution. Two features were studied in detail, deformation bands within the sandstones as indicators for compaction and veins within the overlying Etendeka volcanic rocks as indicators of fluid flow conditions.

2. Geologic Setting

The geology of the study area in Namibia is characterized by Neoproterozoic basement of the ~N-S trending Kaoko belt, an orogenic belt which formed during the assemblage of

Gondwana (e.g., Goscombe et al., 2005; Foster et al., 2009; **Fig. 1a**). These metamorphic rocks are covered by the sedimentary rocks of the Karoo Supergroup that were deposited across large parts of southern Africa and South America in an intracontinental basin (de Wit et al., 1988; Smith et al., 1993). In the studied Huab Basin the Karoo units comprise mostly lake deposits with a thickness of around 180 m, which varies due to the basement topography (Horsthemke, 1992; **Fig. 2**). The Karoo rocks are superposed by the Twyfelfontein Formation, an aeolian sandstone of Lower Cretaceous age (e.g., Scherer, 2000; Dentzien-Dias et al., 2007; Perea et al., 2009). In the Huab Basin, this sandstone formation reaches a thickness of up to 100 m (Miller, 2008) and inter-fingers with the basal units of the Paraná-Etendeka volcanic rocks (Jerram et al., 1999; Stanistreet and Stollhofen, 1999; **Fig. 2**). The latter extruded at 133 ± 1 Ma (Renne et al., 1992) and the eruptions span across approximately 2.4 Ma (Milner et al., 1995) and thus happened shortly before or during the onset of Atlantic rifting at this latitude (e.g., Bauer et al., 2000; Blaich et al., 2011; Stica et al, 2014). At present, a maximum thickness of 700 m is preserved in NW Namibia, yet the volcanic rocks must have had a minimum thickness of 1800 m in order to cover the prominent Brandberg granite pluton, which intruded into the Etendeka volcanic rocks contemporaneously or shortly after their emplacement (Watkins et al., 1994; Schmitt et al., 2000) and is situated a few kilometers south of our study area. Thermochronological data indicate a thickness of up to 3000 m (Raab et al., 2005), however this value varies significantly with the assigned paleotemperature and the authors emphasize that the calculated thickness may be too high. To the present knowledge, no further deposits have been emplaced above the volcanic rocks.

3. Methodology

This work is conducted with the combination of field work, optical and scanning electron microscopy and chemical analysis. We studied 24 outcrops of Twyfelfontein sandstone in the Huab Basin that contained deformation bands and measured the orientation, thickness and amount of displacement along the bands and collected around 20 samples. Oriented samples were picked from outcrop walls and additional samples were taken from loose rocks on the ground in order to not cause inappropriate damage. In the overlying basalts, we collected samples of veins in one outcrop near the Bergsig Fault that cuts through the volcanic rocks in the Etendeka Plateau (**Fig. 1**).

Six thin sections of deformation bands were cut perpendicular to the bands, after being impregnated in epoxy to ensure no loss of material. Three thin sections were cut from two vein samples, N-56 and N-56-2. Two of these thin sections derive from a vertical and horizontal face of the vein of sample N-56 to gain knowledge about the shape and orientation of comprised wall rock fragments. Polished thin sections of the samples were analyzed with an optical and a scanning electron microscope. Electron microscopy, i.e. secondary electron, backscatter electron, and cathodoluminescence imaging was conducted on a FEI Quanta 200F scanning electron microscope. Spectral analysis via backscatter electron imaging was conducted using the software EDAX Genesis 5.3. The setup further allowed mapping of the distribution of chemical elements, which we used for visualizing mineral distributions in the veins. Raman spectroscopy on a HORIBA Jobin Yvon HR800 was used to determine vein minerals.

Porosity measurements of the deformation band samples were conducted using 2D image analysis. It is assumed that the 2D porosity is approximately equal to 3D porosity (Johansen et al., 2005). Stitched cathodoluminescence, backscatter electron and secondary electron images of 90x magnification were used to determine the extent of the deformation band. The porosity

analysis was conducted using Adobe Photoshop and the 2D image analysis software ImageJ. A binary image of each sample was created with this software to allow for differentiation between pore space and surface area. To reduce errors, the binary image was manually altered by removing artificial objects such as epoxy vesicles, which the software had recognized as surface area. We therefore regard the error as minimal. The porosity is then determined by counting pixels of pore space and surface area within band and host rock. To visualize porosity changes in the sample, we set a 1 mm-grid across the binary image and calculated the porosity for each 1 mm square. Depending on the porosity, a different color was assigned to the respective square. To determine the effect of grain crushing, cementation and clay input on the porosity, each feature was cropped manually using Adobe Photoshop. This allowed to measure the porosity change from host rock to deformation band due to initial grain crushing, the porosity change induced by cementation, and the porosity change induced by clay input.

4. Results

4.1 Field Data

In the field, we measured the orientation of 399 deformation bands which we found in all of 24 outcrops of the Twyfelfontein Formation (**Fig. 1, 3)**. Deformation bands occurred in both coarse- and fine-grained, and laminated and thick-bedded sections of the sandstone. Their dominant strike is NNW-SSE which is parallel to the present continental margin offshore Namibia and they have an average dip of 60-80° (**Fig. 3f,** for separated outcrop stereograms see appendix). Deformation bands appear as single bands or conjugated pairs. Conjugated bands usually intersect at angles of around 35-40° (**Fig. 3**). Offsets along the bands range from zero to 40 cm and thicknesses vary between 1 and 30 mm, however no correlation between the thickness and the amount of offset is evident (data are shown as supplementary material). Except for two bands with a minor reverse shear sense, offsets are usually normal.

Veins in the Etendeka volcanic rocks have been found in basaltic rock in a prominent ~50 km long N-S trending valley hosting the Bergsig Fault (**Fig. 1**). The veins appear as mode I fractures and have lengths of up to 10 m and widths of up to 25 mm. Along a ~200 m-long river-bed outcrop, they occur in clusters over zones of ~15-100 cm in which some veins intersect each other multiple times (**Fig. 4**). The veins dip steeply with dips >80° and strike directions are NNW-SSE and E-W (**Fig. 4**). Similar veins have also been found near a normal fault at the western edge of the Etendeka Plateau, but are otherwise absent in the volcanic rocks, and thus appear to be related to faulting.

4.2 Thin Sections of Deformation Bands

We analyzed six deformation bands in detail and their description is summarized in **table 1**. Examples of deformation bands on plane polarized and cross polarized light photomicrographs are shown in **figure 5** and on secondary electron and cathodoluminescence images in **figure 6**. Four samples comprise moderately to well-sorted quartz arenites and two are quartz wackes with poor and moderate grain sorting (**table 1**). The clay content in the quartz arenites is around 2-5 % and in the quartz wackes around 15-20 %. It is apparent that the well sorted host rocks produced cataclastic bands, whereas the poor to moderately sorted host rocks produced disaggregation bands. This is in general consensus with other studies (Fossen et al., 2007, and references therein). Half of the sampled deformation bands comprise an offset of 1 cm, while the other half does not show an offset, regardless of the type of band. A porosity reduction of the bands is observed especially in the cataclastic bands (**table 2, Fig. 7**). The porosity in cataclastic bands is

significantly lower (0.03 to 0.09) than in the host rock (0.08 to 0.19), while porosity is only slightly lower or even higher in the disaggregation bands (0.10 and 0.10 in the band versus 0.13 and 0.09 in the host rock) (**Fig. 7**). This observation is also in agreement with previous studies (Fossen et al., 2007, and references therein).

4.3 Sample N-72-1

Best images were obtained from sample N-72-1, which is a quartz arenite that comprises a cataclastic band porosity of 0.03 and a host rock porosity of 0.10 (**table 2**). In secondary electron images, the band is visible as a compact structure with highly irregular grain boundaries, yet on cathodoluminescence images it is obvious that the grains are heavily fractured and shattered within the deformation band (**Fig. 6a**). Fracturing of quartz grains also occurs outside the band, although not nearly as extensive as within the band. Space between the fragments is cemented with quartz, which is responsible for the compact appearance of the band on secondary electron images. Quartz cementation that is filling fractures and pore space along intact quartz grains is also evident outside the band. Pressure solution features, i.e. micro-stylolites, are present, which dissolve both quartz grains and quartz cement (**Fig. 8**). Small open fractures are scattered throughout the sample, some of which offset the cemented ones (**Fig. 8a**). We mapped the orientation of cemented and open fractures outside the band, as well as micro-stylolites in the whole thin section. A length-azimuth rose plot reveals a favored orientation of the cemented fractures of around 40° relative to the deformation band (**Fig. 9**). The open fractures show in general a larger scatter in orientation, although their orientation maximum is also around 40° relative to the orientation of the deformation band (**Fig. 9**). This maximum, however, is guided by the cemented fractures since many of the open fractures re-opened the cemented ones. Micro-stylolites formed preferentially in horizontal orientation (**Fig. 9**).

As the cementation fills up most of the space between the fragments in the deformation band, it is clear that it contributes significantly to the low porosity in the band. However, this is also true for the host rock where cementation is present as well. We analyzed the influence of cementation and deformation band formation on the porosity separately as outlined in **chapter 3**. Prior to the cementation, the host rock and the deformation band had a porosity of 0.23 and 0.15(**Fig. 10a**). After the cementation, the porosity is 0.13 in the host rock and 0.05 in the band (**Fig. 10b**). The clay fraction reduces the porosity to 0.10 (host rock) and 0.03 (band) (**Fig. 10c**), which leads to the 70 % porosity reduction shown in **table 2**. A factor that is not implemented is the pressure solution. As the micro-stylolites formed after the cementation, the porosity values of host rock and band prior to the pressure solution represent minimum values. Further, the pressure solution has probably added to the porosity difference between host rock and deformation band, due to the increased presence of micro-stylolites in the deformation band (0.47 mm stylolite length per mm² in band versus 0.20 mm stylolite length per mm² in host rock; **Fig. 9**). Here, the cementation resulted in an increased amount of grain boundaries along which the pressure solution could take place.

4.4 Thin Sections of Basalt Veins

Thin sections were cut from two samples whose macroscopic texture is similar to the other veins in the Bergsig valley outcrop and at the western edge of the Etendeka plateau, and are therefore regarded as representative. The vein of sample N-56 shows a large content of elongated basalt fragments of which most are aligned approximately parallel to the wall rock. Their appearance in both the vertical and horizontal thin section suggests a disc-like structure. The vein of sample N-56-2 contains fragments that are blocky, yet elongated fragments also occur (**Fig. 11**).

The veins are filled with an abundance of quartz with a colloform and moss texture (after Adams, 1920, and Dong et al., 1995). The remaining cavities have been filled with zeolites, i.e. stilbite and mordenite in sample N-56 (**Figs. 12a, b**) and an unidentified zeolite in N-56-2 (**Fig. 12c**). In sample N-56, the moss quartz has a slight euhedral quartz overgrowth where it is in contact with stilbite (**Fig. 12a**).

5. Discussion

5.1 Diagenetic evolution of the Twyfelfontein sandstone

From the observed features in sample N-72-1, a clear evolution of diagenetic processes is evident. The first step is the formation of deformation bands by grain crushing, which is followed by step two, the growth of the quartz cement. The third step is the formation of micro-stylolites, which are younger than the cement since the latter is dissolved along the stylolites (**Fig. 8a**). The last step is the formation of open fractures. The exact timing of the clay input is unclear, as the clay could have been present since the sedimentation or transported into the rock by fluids at a later stage. We think that the evolution of the different diagenetic processes in the sandstones and their deformation bands is associated with the following events: The formation of the deformation bands (localized grain crushing or sliding) is most likely related to opening of the South Atlantic and emplacement of the basalts. This is emphasized by the preferred orientation of the bands parallel to the continental margin (**Figs. 1, 3**). Syn-volcanic and rift-related faulting is also argued for by Milner and Duncan (1987) and Salomon et al (2015a). The cemented fractures outside the deformation band probably developed simultaneously to the band as a conjugated fracture set as this narrow angle is in accordance to the angle of conjugated deformation bands in the field (**Figs. 3**, **4**).

The next successive step after the brittle formation of the bands is the growth of the quartz cement, which is dependent on a number of factors, such as fluid composition and pH, rock composition and rock fabric (Worden and Morad, 2000). An important control on the rate of quartz cementation is temperature (Walderhaug, 1994). A minimum of 70°C is thought to be necessary to start cementation and the cementation rate increases significantly with increasing temperature (e.g., Rimstidt and Barnes, 1980; Bjørlykke and Egeberg, 1993; Oelkers et al., 1996; Lander and Walderhaug, 1999). In our study area, temperature may also be the key factor on controlling the rate of cementation. That cementation has not started prior to deformation band formation is most likely related to the restricted burial depth of the rock, i.e. a maximum burial depth of 100 m prior to the extrusion of the Etendeka volcanic rocks is too low for a geothermal temperature exceeding 70°C. In addition, the rock may not have been fluid-saturated, because the sandstone was deposited in a desert environment and the groundwater level was probably low. Only with the emplacement of the Etendeka extrusive rocks, the sandstone was buried to greater depths and reached its maximum burial depth with the end of the extrusion. An increased geothermal gradient due to the volcanic activity should have resulted in a high rate of quartz cementation. The quartz cement was not derived from the pressure solution present in the sample, as the micro-stylolites are younger than the cement. The silica needed for the cement must have therefore been transported into the sampled rock. This is also suggested by Dickinson and Milliken (1995) who observe that pressure solution in the Twyfelfontein sandstone cannot provide enough silica for the amount of cement. Hydrothermal fluid circulation is plausible during volcanic activity and could therefore be responsible for the transport of silica from greater depth, into the sampled rock. This is supported by Bjørlykke (2014) who argues that only hydrothermal circulation can provide enough advective silica to allow significant quartz

precipitation in sandstone. Hence, we argue that the cementation is linked to the extrusion phase of the Etendeka lavas.

At some point in time, quartz cementation stopped and stylolite formation started. The reason for the end of quartz cementation could be rooted in the geothermal gradient that may have decreased to a normal gradient after volcanic activity. The micro-stylolites are most likely related to gravitational burial stress, as evident from their preferred horizontal orientation (**Fig. 9**). Stylolite formation, i.e. pressure solution, is generally dependent on factors such as the effective stress acting on the quartz grains (Gratier et al., 2005), fluid saturation and flux (Renard et al., 2000; Taron and Elsworth, 2010). The effective stress is the difference between the lithostatic and hydrostatic pressure. Hydrothermal fluid circulation increases the hydrostatic pressure and therefore reduces the effective stress. This could serve as an explanation for the observation that micro-stylolites occur only after the precipitation of the quartz cement: during hydrothermal circulation that led to the precipitation of the cement, the effective stress may have been reduced to a degree where pressure solution could not take place. Further, the hydrothermal fluid was supersaturated with silica as it was responsible for the quartz precipitation. Thus, the fluid may have been saturated with silica up to a level which prevented pressure solution. After volcanic activity, the fluid pressure decreased, but the lithostatic pressure remained high because of the persisting rock overburden, leading to an effective stress where stylolites could form. On the other hand, stylolites may initially grow slowly (Koehn et al., 2012) and it may therefore be that micro-stylolites that grew at an early stage during the fast cementation cannot be seen in the sample.

5.2 Porosity reduction

The creation of cataclastic bands in the investigated samples results in a significant reduction of porosity with respect to the host rock (**table 2, Fig. 7**). The separation of cement from the grains and grain fragments show that the cementation reduces porosity by a slightly larger amount as the crushing of grains (**Fig. 10**). Sole grain crushing leads to a reduction of 0.08 and the cementation to reduction of 0.10 in both band and host rock. Hence, the cementation within the band is the reason for the development of compaction band seals that hinder fluid flow across these structures.

Micro-Stylolites tend to occur more often within the band than in the matrix (**Fig. 9**). The cemented band acts as a hard rock that can only deform by pressure solution, since no pore space is present to accommodate relative grain displacement. In addition, the crushed grain boundaries provide fresh surfaces where dissolution can take place relatively easily. This implies that pressure solution results in more compaction within the bands than outside, which induces an additional component of movement along the deformation band. Consequently, the offset produced along a deformation band is a two-step process. First, the initial formation of the band, i.e. the grain crushing, produces the largest portion of offset. This process is mainly brittle and happens over a short time period, as shown in rock deformation experiments (Baud et al., 2012). Second, when the band is cemented and stylolites develop, pressure solution, as a ductile-time dependent process, contributes to the offset on a longer time scale. This process will be reaction or diffusion limited and as such relatively slow. Because the stylolites are oriented at an oblique angle to the bands, pressure solution leads to band thinning.

5.3 Fault veins in the Etendeka volcanic rocks

The two analyzed veins in the Etendeka volcanic rocks contain mostly elongated basaltic wall rock fragments (**Fig. 11**). The elongated chips may be the result of thermal spalling, which occurs when rock surfaces are heated quickly (Preston and White, 1934; Walsh and Lomov,

2013). Due to the low conductivity of rocks, the heat generates a large temperature gradient from the rock surface towards the rock matrix. The high temperature gradient leads to expansion of the surface causing compression in the adjacent rock, which subsequently creates surface-parallel fractures. Once these fractures are long enough the superficial fragments buckle away from the host rock and are chipped off. The formation of a larger spall may be seen in sample N-56 where a fracture extends in the host rock parallel to the vein in the upper left hand corner (**Fig. 11**). As already emphasized by the observations of cementation in the Twyfelfontein sandstone, a hydrothermal fluid system was most likely present during and shortly after the emplacement of the Etendeka volcanic rocks. These hot fluids may have penetrated into the overlying volcanic rocks and caused spallation of the respective rock. The spallation is not necessarily restricted to the sample location, as the spalls could have been transported upwards during fluid ascent.

The quartz crystal growth shows three different textures: colloform, moss and euhedral. The former two are especially apparent in sample N-56-2, while euhedral quartz occurs only to a minor extent in sample N-56 (**Fig. 12a**). Whereas euhedral quartz forms from a low-temperature hydrothermal fluid, colloform and moss textures are regarded as a clear indicator for a high-temperature hydrothermal fluid (Dong et al., 1995; Moncada et al., 2012; Shimizu, 2014). Quartz with colloform or moss texture is precipitated from a silica gel, a highly supersaturated fluid which develops when a fluid is quickly vaporized or boiled (Dong et al., 1995). Such an effect may occur during a sudden pressure decrease, e.g. induced by the sudden opening of fractures during seismic activity or increased fluid pressure, into which the fluid penetrates (Moncada et al., 2012). This may apply to our study area, as the vein samples are collected close to the Bergsig Fault (**Fig. 1b**). Activity of the fault may have created a sudden pathway for fluids into the volcanic rocks that had been trapped in the Twyfelfontein sandstone. The veins tend to strike NNW-SSE (**Fig. 4**) and might therefore have been formed during the ENE-WSW directed South Atlantic opening (Salomon et al., 2015b).

The vein of sample N-56 shows a late stage closure by the zeolites mordenite and stilbite (**Figs. 12a, b**). Mordenite is a high-silicic zeolite and therefore common in rhyolites or tholeiitic basalts (Coombs et al., 1959; Walker, 1960; Kitsopoulos, 1997), while stilbite, as one of the most abundant zeolites, is very common in mafic rocks (Deer et al. 2004). Both zeolites have also been identified in amygdules of the Paraná-Etendeka volcanic rocks on the Brazilian side (Murata et al., 1987). Whereas mordenite can form within a wide temperature range (Coombs et al., 1959; Deer et al., 2004; Denton et al., 2009), stilbite is a low-temperature zeolite which does not form above ~120-140°C (Parry, 1998; Kiseleva et al., 2001). In the vein it appears that mordenite and stilbite have not formed simultaneously: although both minerals fill cavities bounded by moss quartz, the latter is capped by euhedral quartz only along the stilbite-filled cavities. This indicates that the mordenite may have formed just after the moss quartz precipitation, possibly in the same hydrothermal fluid phase. The stilbite and the small amount of euhedral quartz represent a later, local circulation of fluid within the basalt at reduced temperatures. This late circulation occurred at low fluid pressures, as the stilbite does not grow in newly formed fractures, but only seals existing cavities. The analyzed fractures provided a significant conduit for fluid flow through the fault-neighboring volcanic rocks for only a short time, since the hydrothermal quartz precipitated quickly and consequently reduced permeability of the fractures.

6. Conclusions

Our study of deformation bands in the Twyfelfontein sandstone and veins in the overlying Etendeka volcanic rocks provides insights into the diagenesis of the sandstone and the evolution

of fluid phases. A model of this process is presented in **figure 13**. Prior to the volcanic activity, the sandstone was unlithified and groundwater flowed undisturbed at normal geothermal conditions (**Fig. 13a**). Deformation bands in the sandstone formed during South Atlantic rifting and loading of the sediments due to the extrusion of the Etendeka volcanic rocks (**Fig. 13b**). Cementation of the sandstone occurred after the deformation band formation and during volcanic activity related elevated fluid temperatures, which also increased the hydrostatic pressure (**Figs. 13b, c**). Faulting within the sandstone related to the South Atlantic opening (Salomon et al., 2015b) brackets the cementation and the elevated geothermal gradient to the time of volcanic activity and rifting. After volcanic activity, the fluid temperature dropped below the minimum temperature necessary for cementation, but the ongoing pressure exerted by the volcanic overburden led to the formation of micro-stylolites (**Fig. 13d**).

In the veins within the Etendeka volcanic rocks we interpret the elongated breccia fragments as spalls that were chipped off from the wall rock when a hot fluid entered cold rock. In combination with colloform quartz this is indicative for a hydrothermal fluid that penetrated into the rock. Initial opening of the veins may be associated with activity on the Bergsig Fault close to the sample locality or fracturing may be induced by fluid overpressure in the underlying Twyfelfontein sandstone (**Fig. 13c**). A later cooler fluid phase interacted with the basaltic host rock and precipitated stilbite. This circulation occurred at low fluid pressures as the stilbite fills only cavities and does not grow in newly formed cracks (**Fig. 13d**). In conclusion, both the analysis of deformation bands and veins provide evidence for a hydrothermal fluid system and a later fluid system at normal geothermal conditions.

Porosity analysis of the deformation bands are in agreement with existing studies, showing that cataclastic bands reduce the porosity significantly, while disaggregation bands show no or only a slight porosity reduction. However, detailed analysis of the porosity evolution shows that cementation contributes slightly more to the porosity reduction from band to host rock than grain crushing.

Our study further contributes to the debate on whether or not the South Atlantic rifting at this latitude started during or after the Paraná-Etendeka extrusion (e.g., Courtillot et al., 1999; Bauer et al., 2000; Blaich et al., 2011; Beglinger et al., 2012; Stica et al., 2014). The deformation bands must have formed prior to, and/or during the extrusion and their orientation parallel to the present margin is a clear indicator that rift-related faulting occurred during the extrusion of the Paraná-Etendeka volcanic rocks.

Acknowledgements

We thank the Geological Survey of Namibia and the Palmvag Lodge for permission to work in the ecologically sensitive areas of NW Namibia. Furthermore, we thank Sebastian Wex for assistance during field work. This project was funded by the German Research Foundation (DFG; grant no. KO 2463/8-1) within the priority program SAMPLE (South AtlanticMargin Processes and Links with Onshore Evolution; SPP 1375). The Schürmann Foundation is thanked for several grants to CWP for field expenses.

References

Adams, S.F., 1920. A microscopic study of vein quartz. Economic Geology 15, 623-664.

Antonellini, M.A., Aydin, A., Pollard, D.D., 1994. Microstructure of Deformation Bands in Porous Sandstones at Arches National-Park, Utah. Journal of Structural Geology 16, 941-959

Aydin, A., 1978. Small Faults Formed as Deformation Bands in Sandstone. Pure and Applied Geophysics 116, 913-930.

Baker, J.C., Havord, P.J., Martin, K.R., Ghori, K.A.R., 2000. Diagenesis and petrophysics of the Early Permian Moogooloo sandstone, southern Carnarvon basin, western Australia. AAPG Bulletin 84, 250-265.

Ballas, G., Soliva, R., Sizun, J.-P., Benedicto, A., Cavailhes, T., Raynaud, S., 2012. The importance of the degree of cataclasis in shear bands for fluid flow in porous sandstone, Provence, France. AAPG Bulletin 96, 2167-2186.

Baron, M., Parnell, J., Mark, D., Carr, A., Przyjalgowski, M., Feely, M., 2008. Evolution of hydrocarbon migration style in a fractured reservoir deduced from fluid inclusion data, Clair Field, west of Shetland, UK. Marine and Petroleum Geology 25, 153-172.

Baud, P., Meredith, P., Townend, E., 2012. Permeability evolution during triaxial compaction of an anisotropic porous sandstone. Journal of Geophysical Research: Solid Earth 117, B05203, doi:10.1029/2012JB009176.

Bauer, K., Neben, S., Schreckenberger, B., Emmermann, R., Hinz, K., Fechner, N., Gohl, K., Schulze, A., Trumbull, R.B., Weber, K., 2000. Deep structure of the Namibia continental margin as derived from integrated geophysical studies. Journal of Geophysical Research-Solid Earth 105, 25829-25853, doi:10.1029/2000jb900227.

Beglinger, S.E., Doust, H., Cloetingh, S., 2012. Relating petroleum system and play development to basin evolution: Brazilian South Atlantic margin. Petroleum Geoscience 18, 315-336.

Bjørlykke, K., 2014. Relationships between depositional environments, burial history and rock properties. Some principal aspects of diagenetic process in sedimentary basins. Sedimentary Geology 301, 1-14.

Bjørlykke, K., Egeberg, P.K., 1993. Quartz Cementation in Sedimentary Basins. Aapg Bulletin-American Association of Petroleum Geologists 77, 1538-1548.

Blaich, O.A., Faleide, J.I., Tsikalas, F., 2011. Crustal breakup and continent-ocean transition at South Atlantic conjugate margins. Journal of Geophysical Research-Solid Earth 116, 38, B01402, doi: 10.1029/2010jb007686.

Cashman, S., Cashman, K., 2000. Cataclasis and deformation-band formation in unconsolidated marine terrace sand, Humboldt County, California. Geology 28, 111-114.

Christie, P.A.F., White, R.S., 2008. Imaging through Altantic Margin basalts: An introduction to the sub-basalt mini-set. Geophysical Prospecting 56, 1-4.

Coombs, D.S., Ellis, A.J., Fyfe, W.S., Taylor, A.M., 1959. The zeolite facies, with comments on the interpretation of hydrothermal syntheses. Geochimica Et Cosmochimica Acta 17, 53-107.

Courtillot, V., Jaupart, C., Manighetti, I., Tapponnier, P., Besse, J., 1999. On causal links between flood basalts and continental breakup. Earth and Planetary Science Letters 166, 177-195.

Cukur, D., Horozal, S., Kim, D.C., Lee, G.H., Han, H.C., Kang, M.H., 2010. The distribution and characteristics of the igneous complexes in the northern East China Sea Shelf Basin and their implications for hydrocarbon potential. Marine Geophysical Researches 31, 299-313.

de Ros, L.F., 1998. Heterogeneous generation and evolution of diagenetic quartzarenites in the Silurian-Devonian Furnas Formation of the Parana Basin, southern Brazil. Sedimentary Geology 116, 99-128.

de Wit, M.J., Jeffery, M., Bergh, H., Nicolayson, L. O. , 1988. Geological Map of sectors of Gondwana reconstructed to their position ~150 Ma (with explanatory notes). Scale 1: 1 000 000. American Associaion of Petroleum Geologists, Tulsa, USA.

Deer, W.A., Howie, R.A., Wise, W.S., Zussman, J., 2004. Rock-forming minerals. Volume 4B: Framework silicates: silica minerals, feldspathoids and the zeolites. 2nd edition, Geological Society, Geological Society Publishing House, Bath.

Denton, J.S., Tuffen, H., Gilbert, J.S., Odling, N., 2009. The hydration and alteration of perlite and rhyolite. Journal of the Geological Society, London 166, 895-904.

Dentzien-Dias, P.C., Schultz, C. L., Scherer, M. S. C., Lavina, E. L. C., 2007. The trace fossil record from the Guará Formation (Upper Jurassic), southern Brazil. Arquivos do Museu Nacional, Rio de Janeiro 64, 585-600.

Department of Energy, 2007. Basic research needs for geosciences: Facilitating 21st century energy systems. Office of Basic Energy Sciences, Bethesda, MA.

Dickinson, W.W., Milliken, K.L., 1995. The Diagenetic Role of Brittle Deformation in Compaction and Pressure Solution, Etjo Sandstone, Namibia. Journal of Geology 103, 339-347.

Dong, G., Morrison, G., Jaireth, S., 1995. Quartz textures in epithermal veins, Queensland - Classification, origin, and implication. Economic Geology and the Bulletin of the Society of Economic Geologists 90, 1841-1856.

Fossen, H., Schultz, R.A., Shipton, Z.K., Mair, K., 2007. Deformation bands in sandstone: a review. Journal of the Geological Society 164, 755-769.

Foster, D.A., Goscombe, B.D., Gray, D.R., 2009. Rapid exhumation of deep crust in an obliquely convergent orogen: The Kaoko Belt of the Damara Orogen. Tectonics 28, TC4002, doi:10.1029/2008tc002317.

Gallagher, J.W., Dromgoole, P.W., 2007. Exploring below the basalt, offshore Faroes: a case history of sub-basalt imaging. Petroleum Geoscience 13, 213-225.

Goscombe, B., Gray, D., Armstrong, R., Foster, D.A., Vogl, J., 2005. Event geochronology of the Pan-African Kaoko Belt, Namibia. Precambrian Research 140, 103-131.

Gratier, J.P., Muquet, L., Hassani, R., Renard, F., 2005. Experimental microstylolites in quartz and modeled application to natural stylolitic structures. Journal of Structural Geology 27.

Horsthemke, E., 1992. Fazies der Karoosedimente in der Huab-Region, Damaraland, NW-Namibia. Göttinger Arbeiten zur Geologie und Paläontologie, v. 55, p. 1-102.

Jerram, D., Mountney, N., Holzförster, F., Stollhofen, H., 1999. Internal stratigraphic relationships in the Etendeka Group in the Huab Basin, NW Namibia: understanding the onset of flood volcanism. Journal of Geodynamics 28, 393-418.

Jin, Q., Xiong, S.S., Lu, P., 1999. Catalysis and hydrogenation: volcanic activity and hydrocarbon generation in rift basins, eastern China. Applied Geochemistry 14, 547-558.

Johansen, T.E.S., Fossen, H., Kluge, R., 2005. The impact of syn-faulting porosity reduction on damage zone architecture in porous sandstone: an outcrop example from the Moab Fault, Utah. Journal of Structural Geology 27, 1469-1485.

Kiseleva, I., Navrotsky, A., Belitsky, I., Fursenko, B., 2001. Thermochemical study of calcium zeolites-heulandite and stilbite. American Mineralogist 86, 448-455.

Kitsopoulos, K.P., 1997. The genesis of a mordenite deposit by hydrothermal alteration of pyroclastics on Polyegos Island, Greece. Clays and clay minerals 45, 632-648.

Koehn, D., Ebner, M., Renard, F., Toussaint, R., Passchier, C.W., 2012. Modelling of stylolite geometries and stress scaling. Earth and Planetary Science Letters 341-344, 104-113.

517 Kristensen, M.B., Childs, C., Olesen, N.Ø., Korstggård, J.A., 2013. The microstructure and
518 internal architecture of shear bands in sand-clay sequences. Journal of Structural Geology
519 46, 129-141, doi:http://dx.doi.org/10.1016/j.jsg.2012.09.015.
520 Lander, R.H., Walderhaug, O., 1999. Predicting porosity through simulating sandstone
521 compaction and quartz cementation. AAPG Bulletin-American Association of Petroleum
522 Geologists 83, 433-449.
523 Lee, G.H., Kwon, Y.I., Yoon, C.S., Kim, H.J., Yoo, H.S., 2006. Igneous complexes in the eastern
524 Northern South Yellow Sea Basin and their implications for hydrocarbon systems. Marine
525 and Petroleum Geology 23.
526 Lima, R.D., De Ros, L.F., 2002. The role of depositional setting and diagenesis on the reservoir
527 quality of Devonian sandstones from the Solimoes Basin, Brazilian Amazonia. Marine and
528 Petroleum Geology 19, 1047-1071.
529 Miller, R.M.G, 2008. The Geology of Namibia, Ministry of Mines and Energy, Geological
530 Survey of Namibia, Windhoek.
531 Milner, S.C., Duncan, A.R., 1987. Geochemical characterisation of quartz latite units in the
532 Etendeka Formation. Communications of the Geological Survey of Namibia 3, 83-90.
533 Milner, S.C., Duncan, A.R., Whittingham, A.M., Ewart, A., 1995. Trans-Atlantic correlation of
534 eruptive sequences and individual silicic volcanic units within the Parana Etendeka igneous
535 province. Journal of Volcanology and Geothermal Research 69, 137-157.
536 Moncada, D., Mutchler, S., Nieto, A., Reynolds, T.J., Rimstidt, J.D., Bodnar, R.J., 2012. Mineral
537 textures and fluid inclusion petrography of the epithermal Ag-Au deposits at Guanajuato,
538 Mexico: Application to exploration. Journal of Geochemical Exploration 114, 20-35.
539 Murata, K.J., Formoso, M.L.L., Roisenberg, A., 1987. Distribution of zeolites in lavas of
540 southeastern Parana Basin, state of Rio Grande do Sul, Brazil. The Journal of Geology 95,
541 455-467.
542 Nadin, P.A., Kusznir, N.J., Cheadle, M.J., 1997. Early Tertiary plume uplift of the North Sea and
543 Faeroe-Shetland Basins. Earth and Planetary Science Letters 148, 109-127.
544 Oelkers, E.H., Bjørkum, P.A., Murphy, W.M., 1996. A petrographic and computational
545 investigation of quartz cementation and porosity reduction in North Sea sandstones.
546 American Journal of Science 296, 420-452.
547 Parry, W.T., 1998. Fault-fluid compositions from fluid-inclusion observations and solubilities of
548 fracture-sealing minerals. Tectonophysics 290, 1-26.
549 Perea, D., Soto, M., Veroslavsky, G., Martínez, S., Ubilla, M., 2009. A Late Jurassic fossil
550 assemblage in Gondwana: Biostratigraphy and correlations of the Tacuarembo Formation,
551 Parana Basin, Uruguay. Journal of South American Earth Sciences 28, 168-179.
552 Preston, F.W., White, H.E., 1934. Observations on Spalling. Journal of the American Ceramic
553 Society 17, 137-144.
554 Raab, M.J., Brown, R.W., Gallagher, K., Weber, K., Gleadow, A.J.W., 2005. Denudational and
555 thermal history of the Early Cretaceous Brandberg and Okenyenya igneous complexes on
556 Namibia's Atlantic passive margin. Tectonics 24, TC3006, doi:10.1029/2004tc001688.
557 Rawling, G.C., Goodwin, L.B., 2003. Cataclasis and particulate flow in faulted, poorly lithified
558 sediments. Journal of Structural Geology 25, 317-331.
559 Renard, F., Gratier, J.P., Jamtveit, B., 2000. Kinetics of crack-sealing, intergranular pressure
560 solution, and compaction around active faults. Journal of Structural Geology 22, 1395-
561 1407.
562 Renne, P.R., Ernesto, M., Pacca, I.G., Coe, R.S., Glen, J.M., Prévot, M., Perrin, M., 1992. The
563 age of Paraná flood volcanism, rifting of Gondwanaland, and the Jurassic-Cretaceous
564 boundary. Science 258, 975-979.

565 Rimstidt, J.D., Barnes, H.L., 1980. The Kinetics of Silica-Water Reactions. Geochimica Et
566 Cosmochimica Acta 44, 1683-1699.
567 Rodriguez Monreal, F., Villar, H.J., Baudino, R., Delpino, D., Zencich, S., 2009. Modeling an
568 atypical petroleum system: A case study of hydrocarbon generation, migration and
569 accumulation related to igneous intrusions in the Neuquen Basin, Argentina. Marine and
570 Petroleum Geology 26, 590-605.
571 Rohrman, M., 2007. Prospectivity of volcanic basins: Trap delineation and acreage de-risking.
572 AAPG Bulletin 91, 915-939.
573 Rohrman, M., 2013. Intrusive large igneous provinces below sedimentary basins: An example
574 from the Exmouth Plateau (NW Australia). Journal of Geophysical Research: Solid Earth
575 118, 4477-4487, doi:10.1002/jgrb.50298.
576 Salomon, E., Koehn, D., Passchier, C., 2015a. Brittle reactivation of ductile shear zones in NW
577 Namibia in relation to South Atlantic rifting. Tectonics 34, 70-85,
578 doi:10.1002/2014tc003728.
579 Salomon, E., Koehn, D., Passchier, C., Hackspacher, P.C., Glasmacher, U.A., 2015b. Contrasting
580 stress fields on correlating margins of the South Atlantic. Gondwana Research 28, 1152-
581 1167.
582 Scherer, C.M.S., 2000. Eolian dunes of the Botucatu Formation (Cretaceous) in southernmost
583 Brazil: morphology and origin. Sedimentary Geology 137, 63-84.
584 Schmitt, A.K., Emmerman, R., Trumbull, R.B., Buhn, B., Henjes-Kunst, F., 2000. Petrogenesis
585 and Ar-40/Ar-39 geochronology of the Brandberg complex, Namibia: Evidence for a major
586 mantle contribution in metaluminous and peralkaline granites. Journal of Petrology 41,
587 1207-1239.
588 Shimizu, T., 2014. Reinterpretation of quartz textures in terms of hydrothermal fluid evolution at
589 the Koryu Au-Ag deposit, Japan. Economic Geology 109, 2051-2065.
590 Shipton, Z.K., Cowie, P.A., 2001. Damage zone and slip-surface evolution over mu m to km
591 scales in high-porosity Navajo sandstone, Utah. Journal of Structural Geology 23, 1825-
592 1844.
593 Shipton, Z.K., Cowie, P.A., 2003. A conceptual model for the origin of fault damage zone
594 structures in high-porosity sandstone. Journal of Structural Geology 25, 333-344.
595 Smith, R.M.H., Eriksson, P.G., Botha, W.J., 1993. A review of the stratigraphy and sedimentary
596 environment of the Karoo-aged basins of southern Africa. Journal of African Earth
597 Sciences 16, 143-169.
598 Stanistreet, I.G., Stollhofen, H., 1999. Onshore equivalents of the main Kudu gas reservoir in
599 Namibia. Geological Society, London, Special Publications 153, 345-365.
600 Stica, J.M., Zalán, P.V., Ferrari, A.L., 2014. The evolution of rifting on the volcanic margin of
601 the Pelotas Basin and the contextualization of the Paraná-Etendeka LIP in the separation of
602 Gondwana in the South Atlantic. Marine and Petroleum Geology 50, 1-21.
603 Taron, J., Elsworth, D., 2010. Constraints on compaction rate and equilibrium in the pressure
604 solution creep of quartz aggregates and fractures: Controls of aqueous concentration.
605 Journal of Geophysical Research-Solid Earth 115, B07211, doi:10.1029/2009jb007118.
606 Torabi, A., 2014. Cataclastic bands in immature and poorly lithified sandstone, examples from
607 Corsica, France. Tectonophysics 630, 91-102.
608 Underhill, J.R., Woodcock, N.H., 1987. Faulting mechanisms in high-porosity sandstones; new
609 red sandstone, Arran, Scotland. Geological Society, London, Special Publications 29, 91-
610 105.

611 Walderhaug, O., 1994. Temperatures of Quartz Cementation in Jurassic Sandstones from the
612 Norwegien Continental-Shelf - Evidence from Fluid Inclusions. Journal of Sedimentary
613 Research Section a-Sedimentary Petrology and Processes 64, 311-323.
614 Walker, G.P.L., 1960. Zeolite zones and dike distribution in relation to the structure of the basalts
615 of eastern Iceland. The Journal of Geology 68, 515-528.
616 Walsh, S.D.C., Lomov, I.N., 2013. Micromechanical modeling of thermal spallation in granitic
617 rock. International Journal of Heat and Mass Transfer 65, 366-373.
618 Watkins, R.T., McDougall, I., Le Roex, A.P., 1994. K-Ar Ages of the Brandberg and Okenyenya
619 Igneous Complexes, North-Western Namibia. Geologische Rundschau 83, 348-356.
620 Worden, R.H., Morad, S. (Eds.), 2000. Quartz Cementation in Sandstones. International
621 Association of Sedimentologists, Special Publication 29, Blackwell Science, Oxford.
622 Wu, C.Z., Gu, L.X., Zhang, Z.Z., Ren, Z.W., Chen, Z.Y., Li, W.Q., 2006. Formation mechanisms
623 of hydrocarbon reservoirs associated with volcanic and subvolcanic intrusive rocks:
624 Examples in Mesozoic-Cenozoic basins of eastern China. AAPG Bulletin 90, 137-147.
625 Wycherley, H.L., Parnell, J., Watt, G.R., Chen, H., Boyce, A.J., 2003. Indicators of hot fluid
626 migration in sedimentary basins: evidence from the UK Atlantic Margin. Petroleum
627 Geoscience 9, 357-374.
628 Zhang, J.X., Wong, T.F., Davis, D.M., 1990. Micromechanics of Pressure-Induced Grain
629 Crushing in Porous Rocks. Journal of Geophysical Research-Solid Earth and Planets 95,
630 341-352, doi:10.1029/JB095iB01p00341.
631
632
633

Figure 1, revised

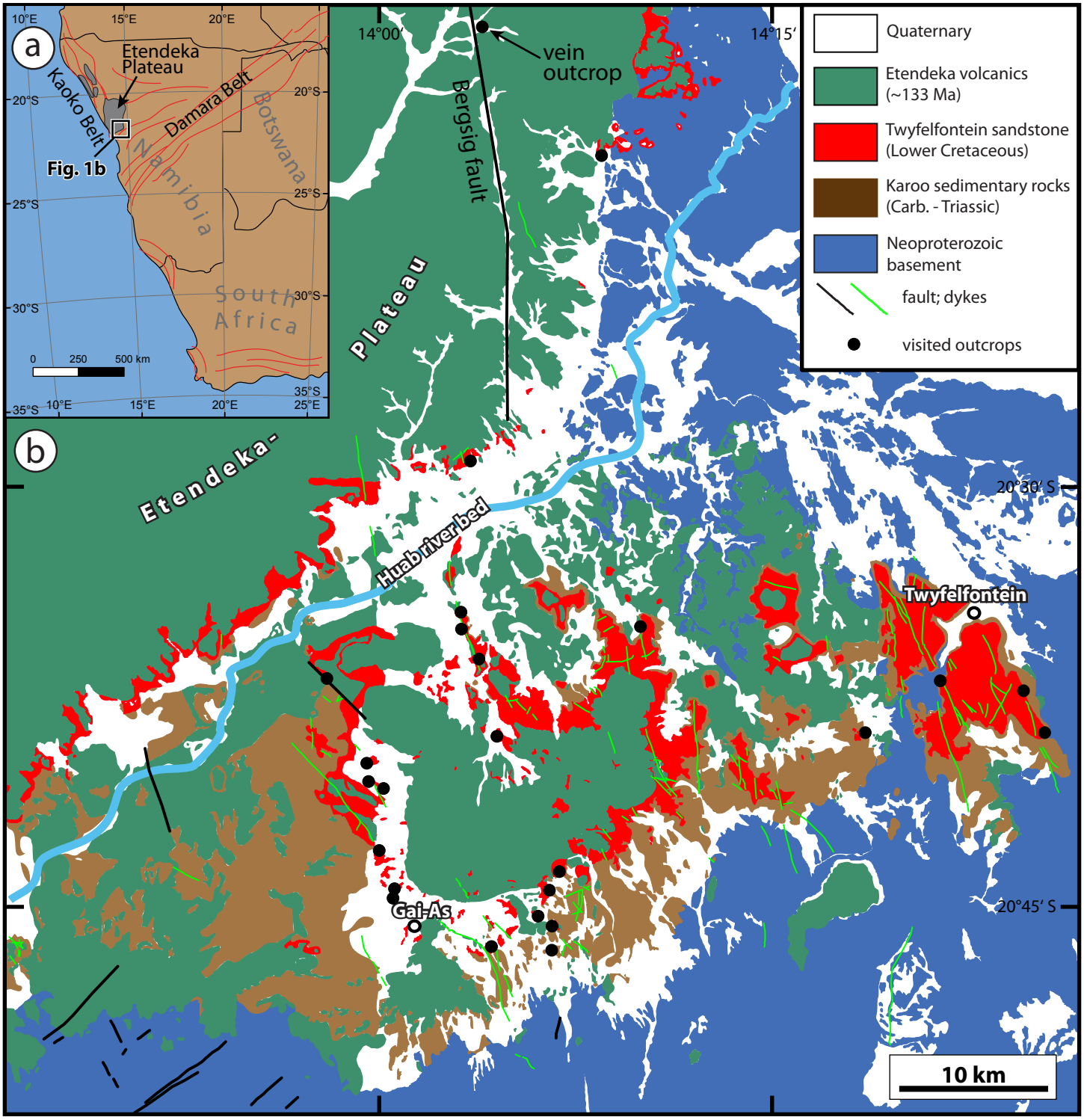

Fig. 1: (a) Map of south-western Africa with location of study area. Red lines indicate trace of Neoproterozoic orogenic belts. Gray areas schematically mark the extent of Etendeka volcanic rocks. (b) Geological map of the study area in the upper Huab basin. Lithology simplified after geological maps „2013 Cape Cross, 1:250.000“ and „2014 Fransfontein, 1:250.000“. Faults and dykes derive from own observations. The outcrop of the sampled veins is located near the northern margin of the map. Location of map shown in (a).

Figure 2

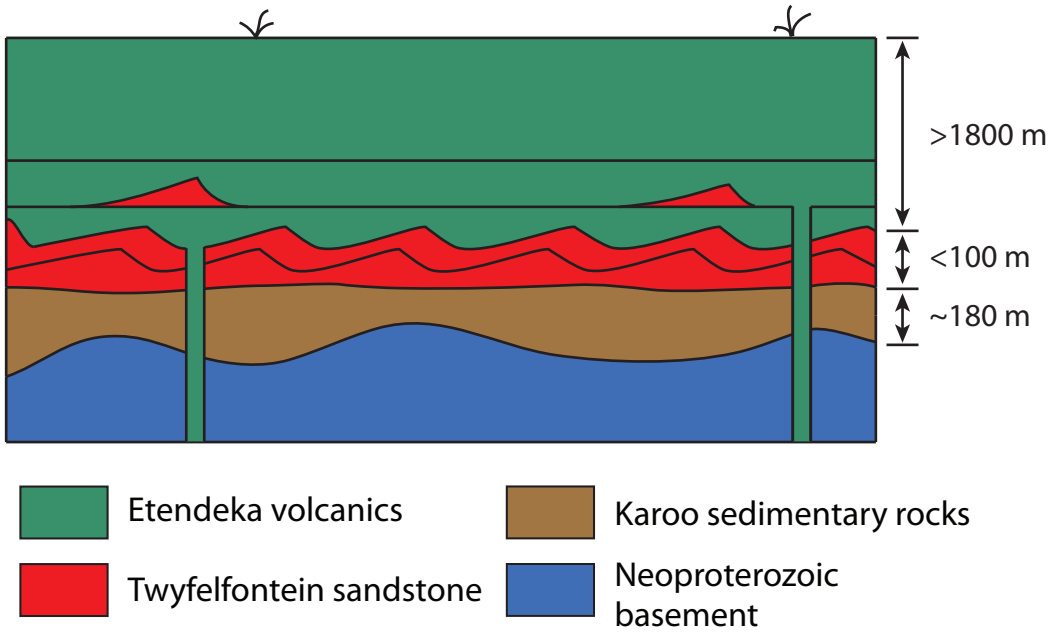

Fig. 2: Schematic stratigraphic profile of the lithology of the Huab Basin. Thickness of Karoo sedimentary rock after Horsthemke (1992) and of Twyfelfontein sandstone after Miller (2008).

Figure 3, revised

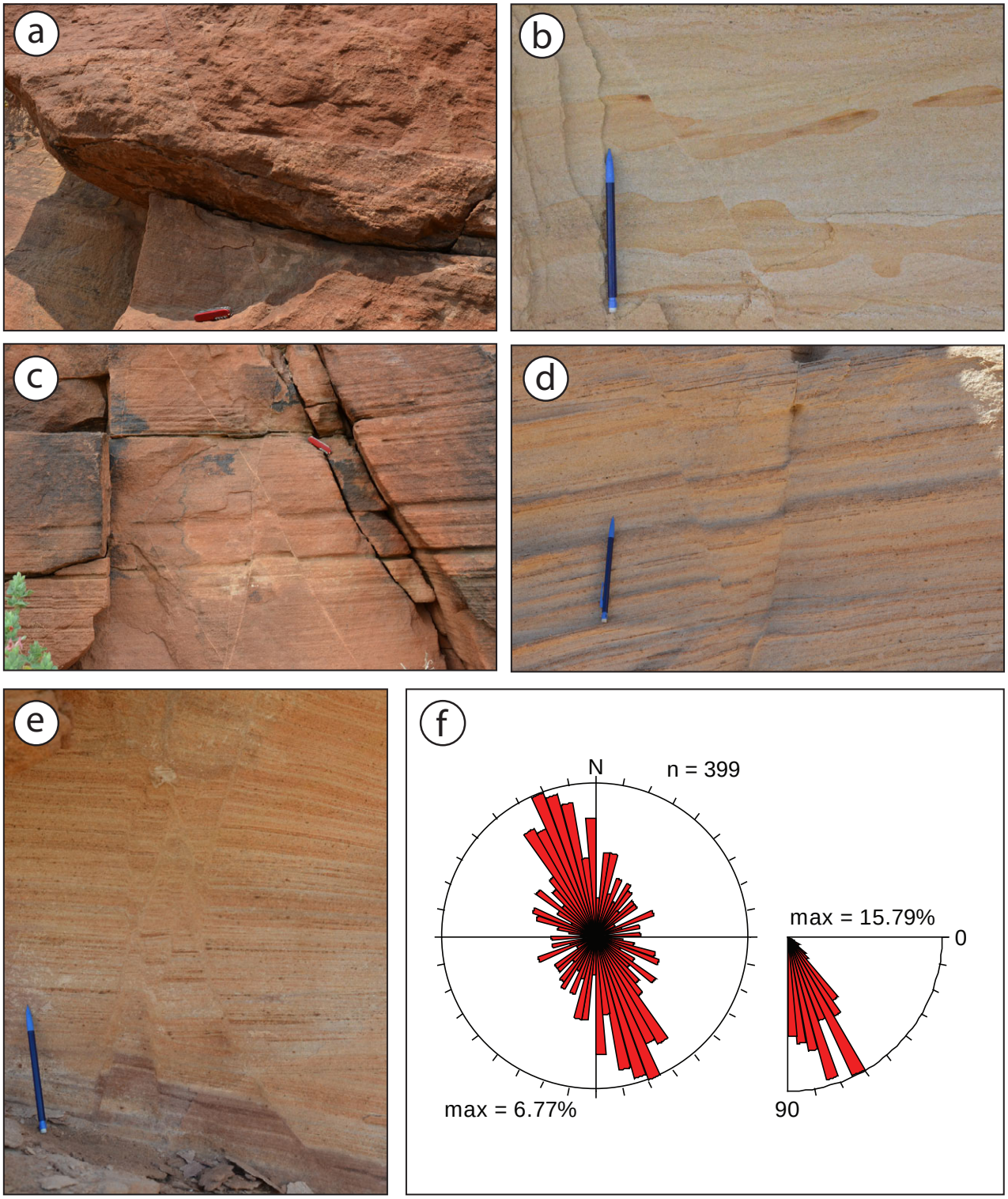

Fig. 3: (a-e) Examples of deformation bands in the Twyfelfontein sandstone. Some bands occur as single bands **(a, b)**, or as conjugated pair **(c-e)**. **(f)** Rose Diagram showing the orientation and dip of the measured deformation bands. Deformation band data are shown as supplementary material.

Figure 4

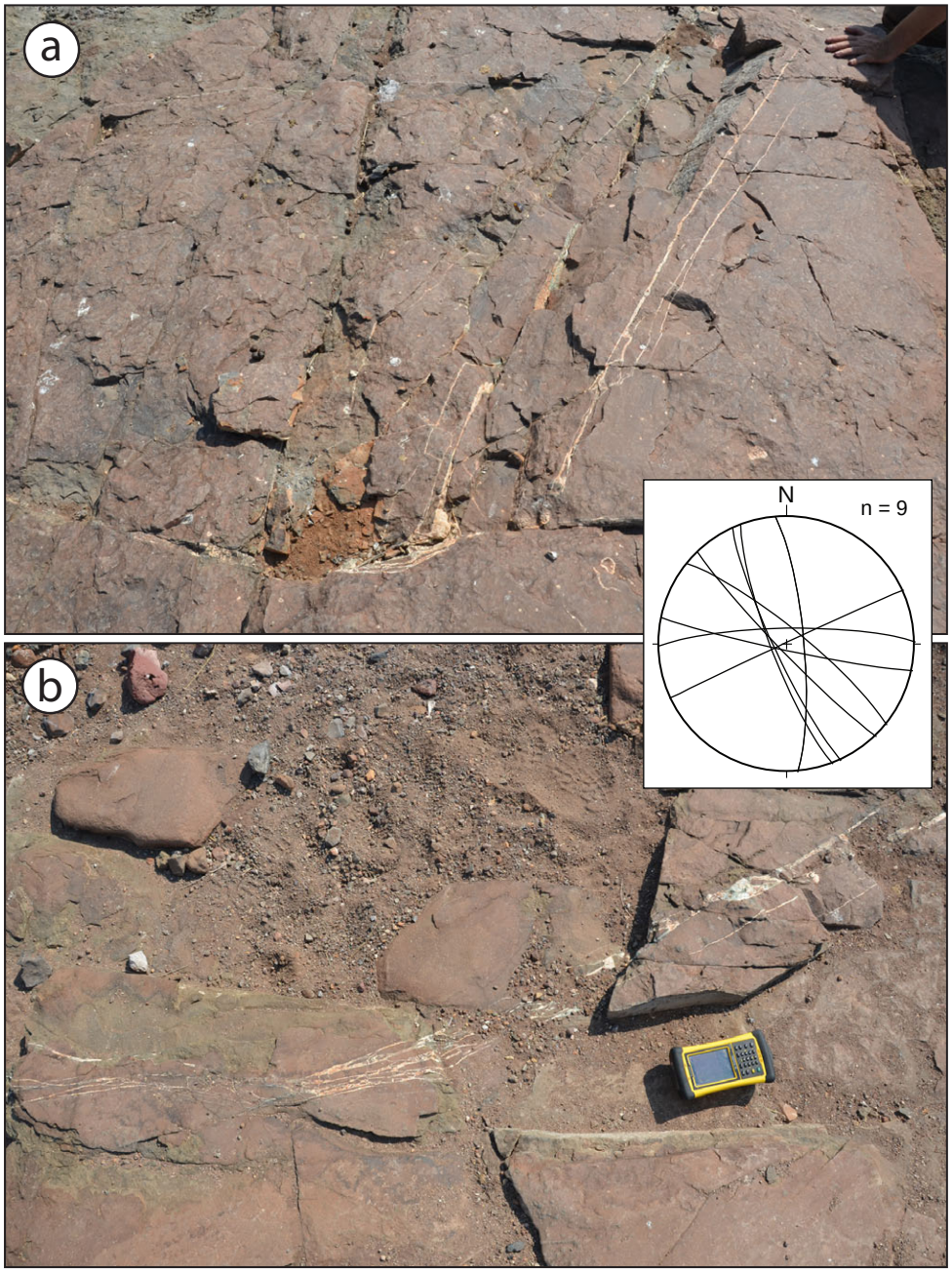

Fig. 4: Sampled veins in the Etendeka volcanics with their orientation shown in stereographic diagram inset.

Figure 5

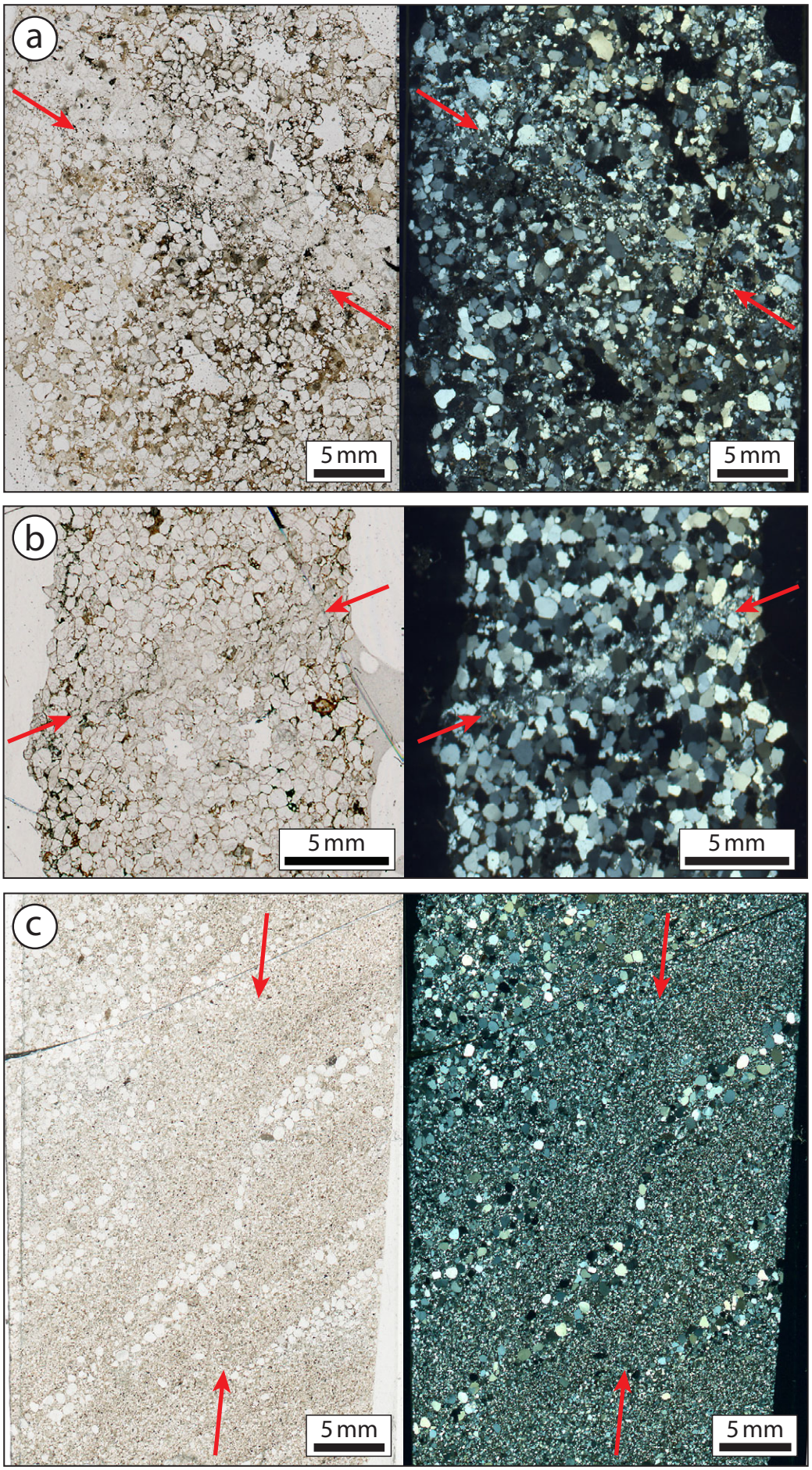

Fig. 5: Plane polarized and crossed polarized light photomicrographs of examples of deformation bands. Trace of deformation band indicated by red arrows. **(a)** cataclastic band of sample N-70; **(b)** cataclastic band of sample N-72-1; **(c)** disaggregation band of sample N-89.

Figure 6

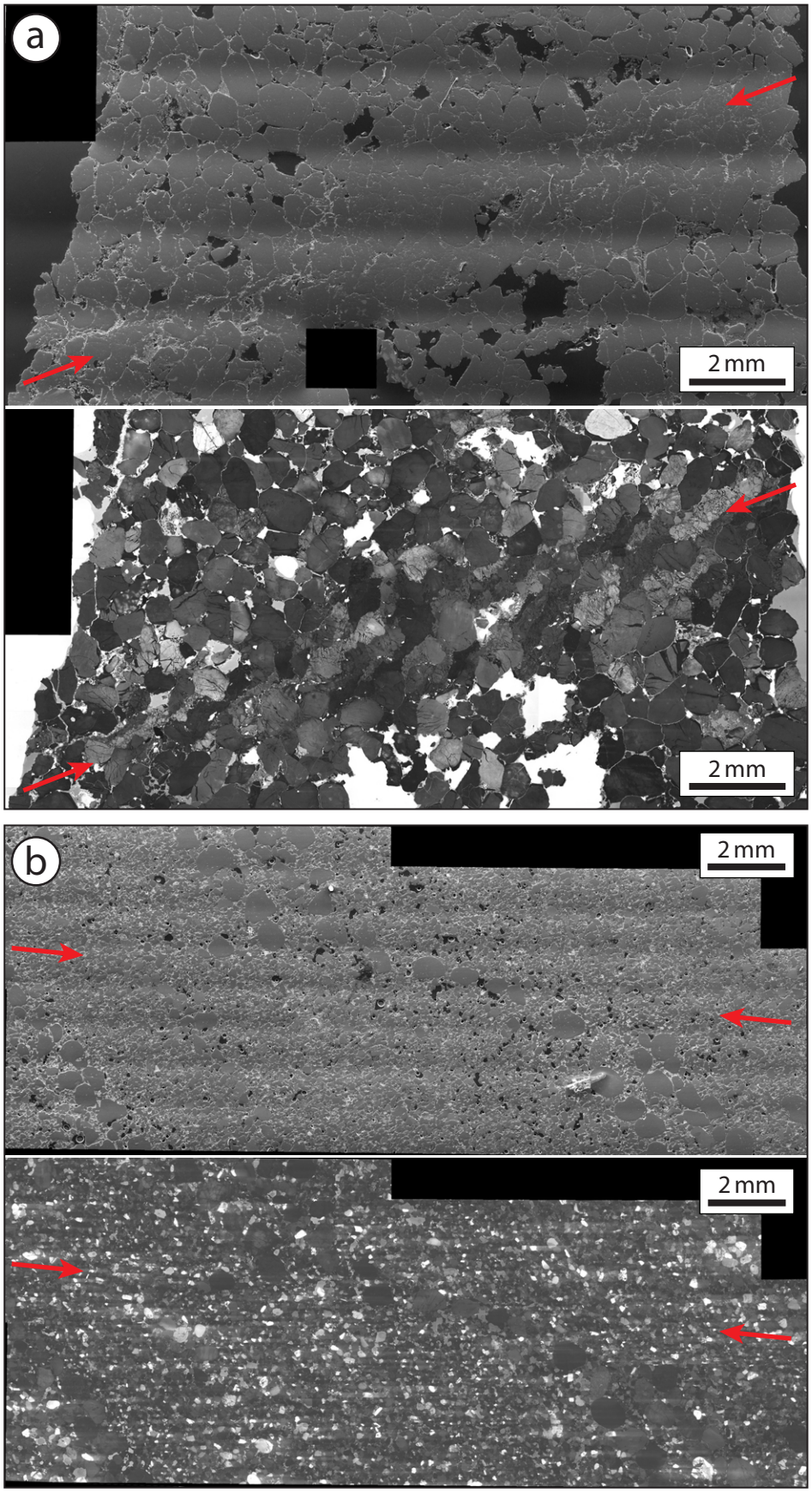

Fig. 6: Examples of a cataclastic band (**a**; sample N-72-1) and a disaggregation band (**b**; sample N-89) on secondary electron and cathodoluminescence images. Trace of deformation bands indicated by red arrows.

Figure 7

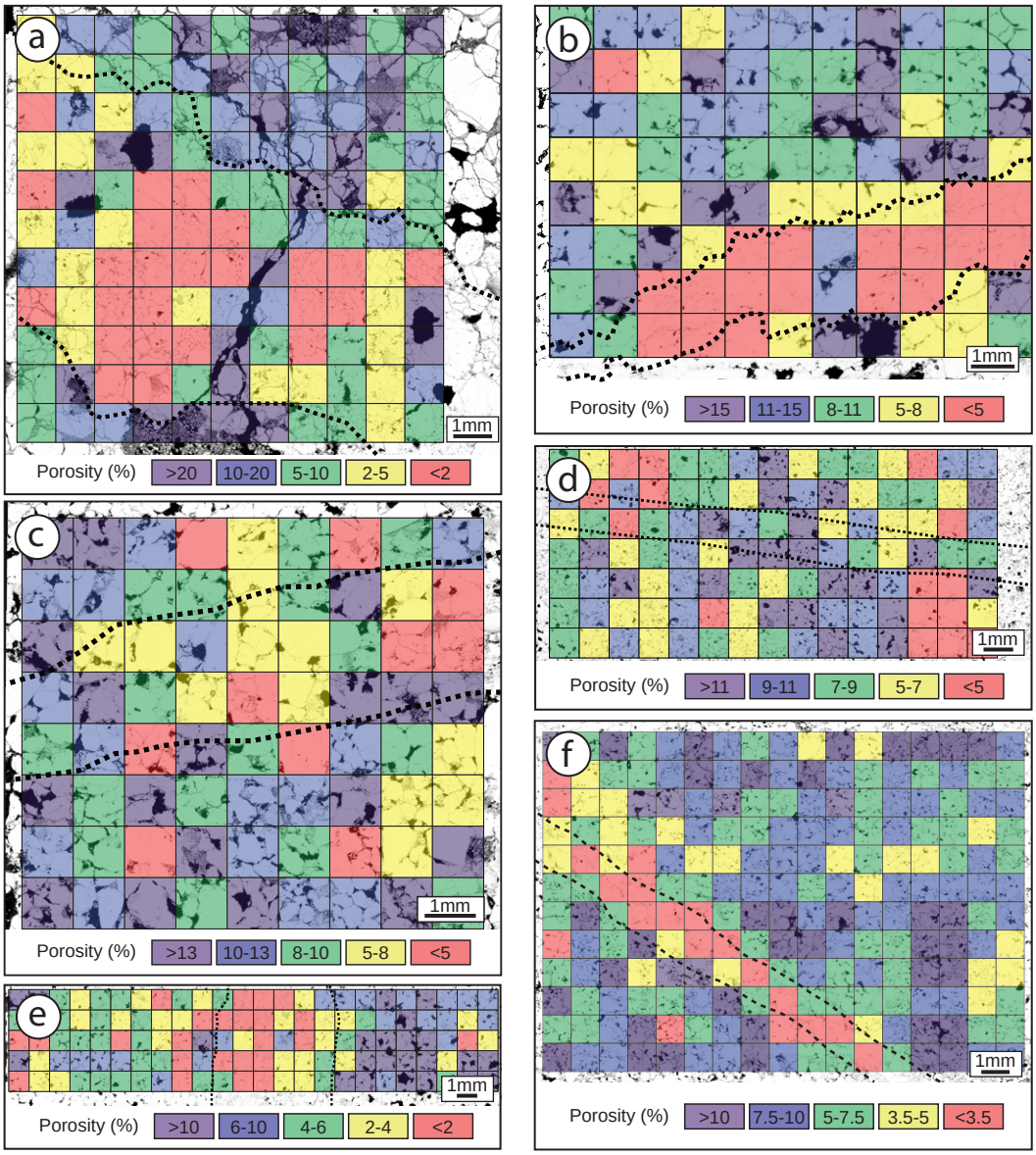

Fig. 7: Porosity maps of deformation bands (within dashed lines) and host rock. Color grid is 1 mm per square and color is assigned to porosity within the respective square. **(a)** sample N-70, **(b)** sample N-72-1, **(c)** sample N-82, **(d)** sample N-89, ***(e)*** sample N-90, **(f)** sample N92.

Figure 8

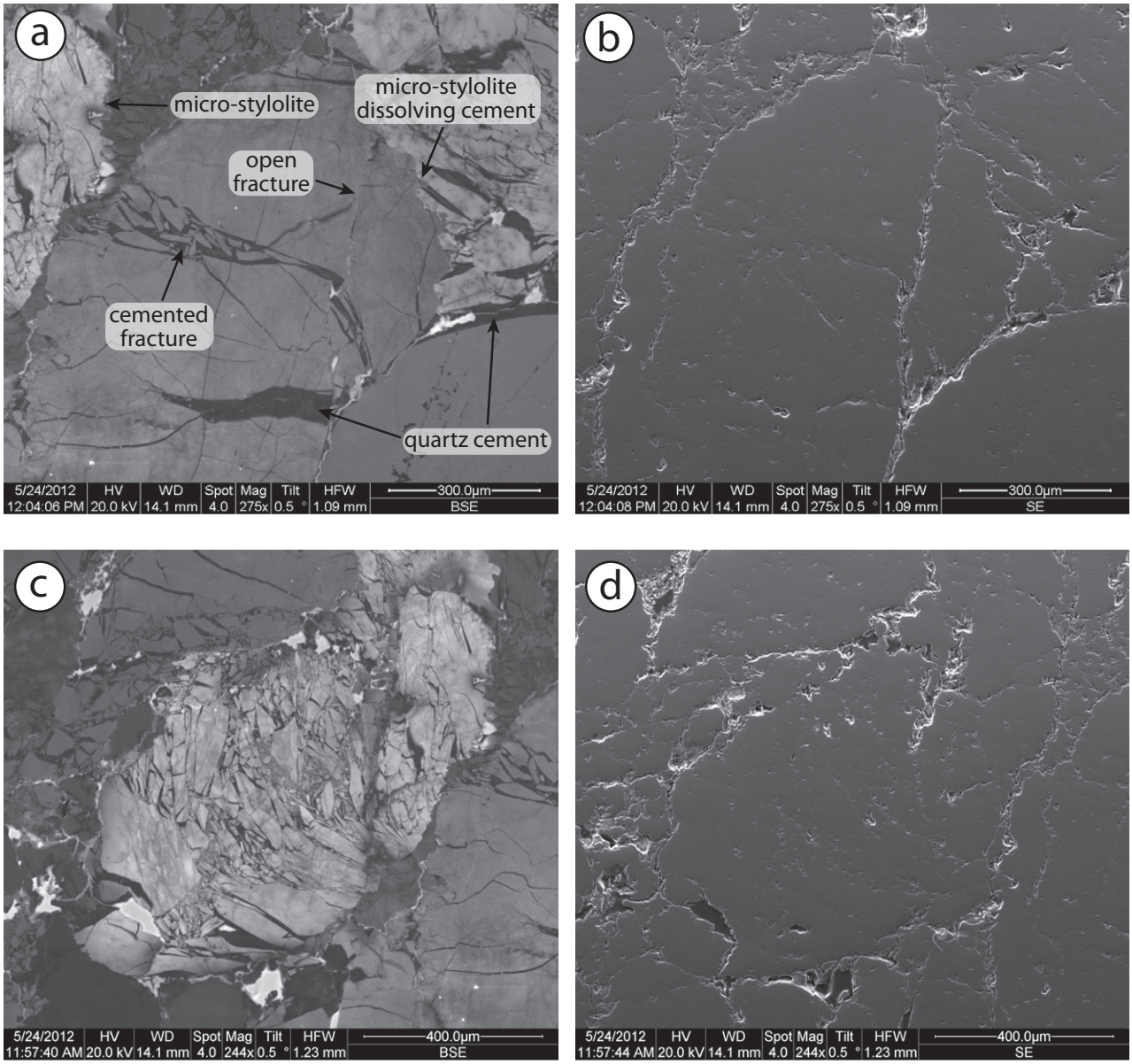

Fig. 8: Detailed cathodoluminescence (CL) and secondary electron (SE) images of fractured grains within deformation band of sample N-72-1. **(a,b)** Initial fractures are filled with quartz cement and the latter is partly dissolved by pressure solution. Open fractures mark a second fracture generation. **(c,d)** Some grains are extensively shattered, yet their original shape is still recognizable.

Figure 9

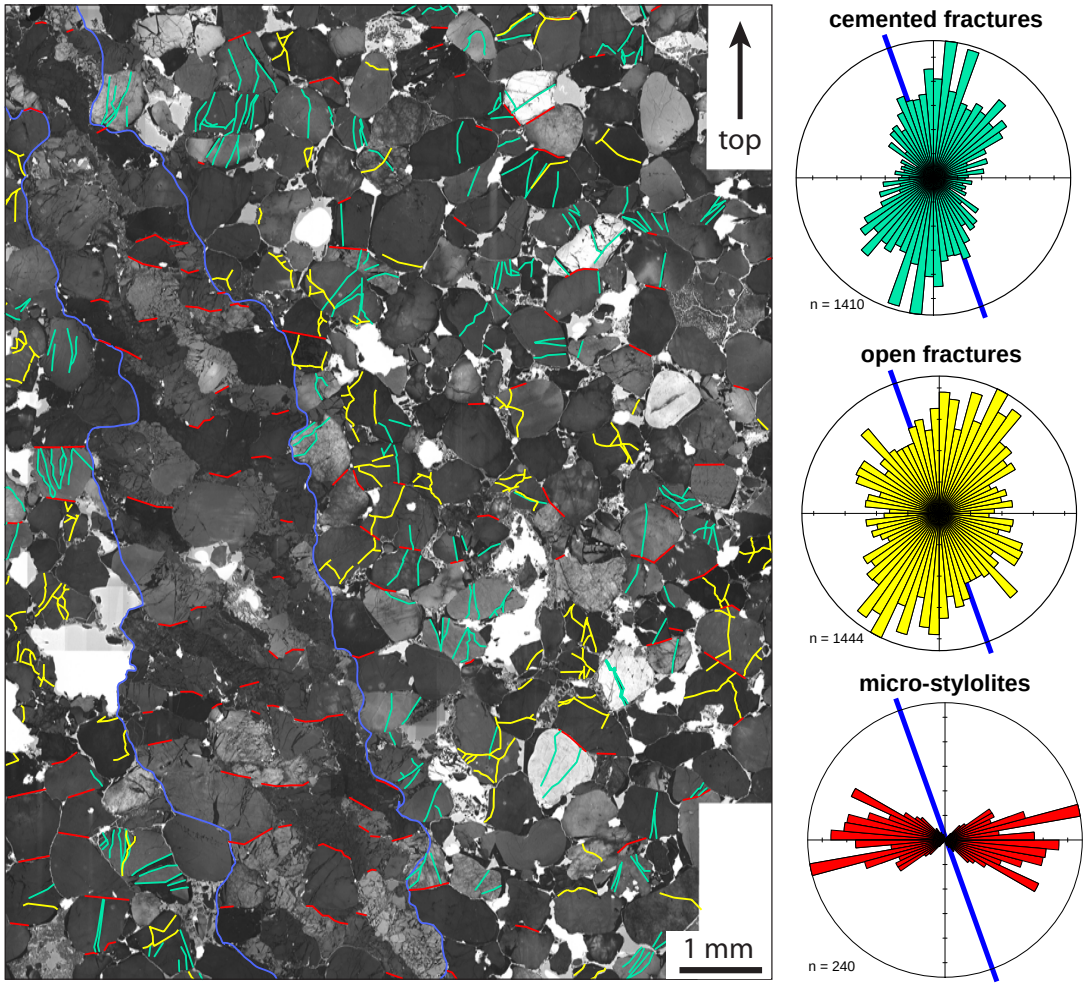

Fig. 9: Orientation of cemented fractures, open fractures and stylolites in sample N-72-1. Fractures are mapped outside the deformation band, whereas stylolites are mapped in the band and host rock. Blue line in rose plots marks orientation of deformation band.

Figure 10, revised

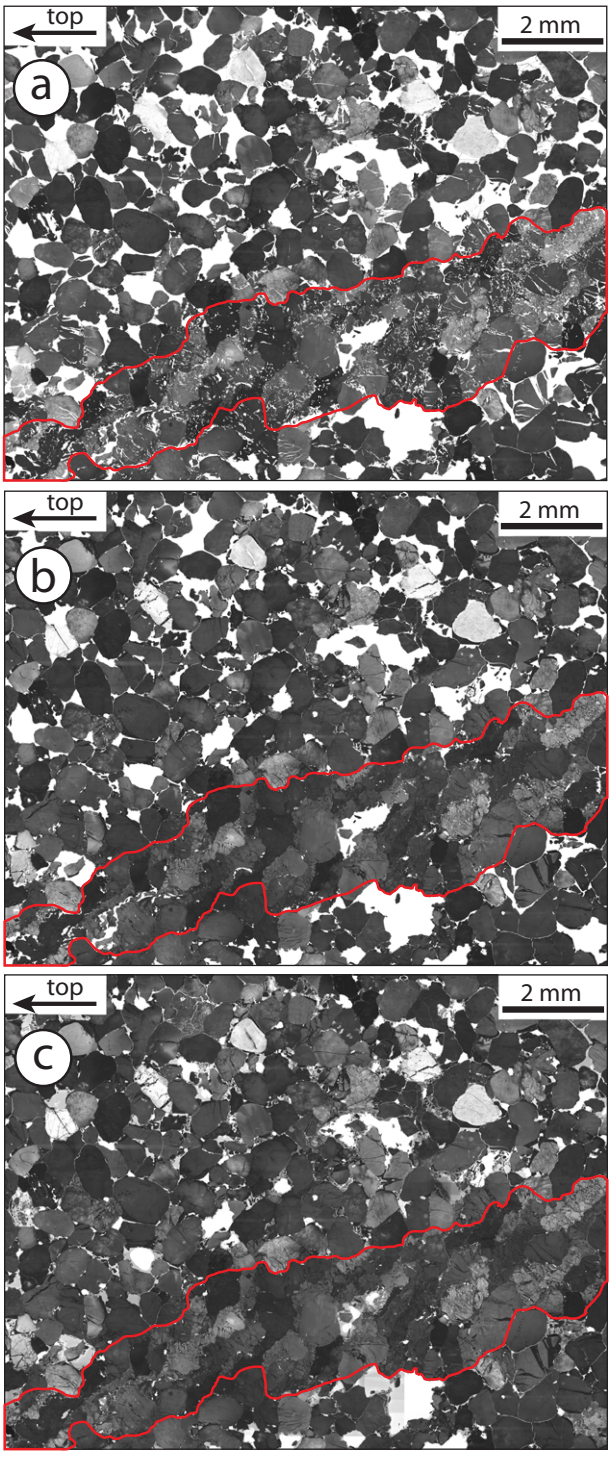

Step 1: formation of deformation band (grain crushing)

Porosity (Φ) in
- host rock: 0.23
- deformation band: 0.15

Step 2: cementation

Porosity (Φ) in
- host rock: 0.13
- deformation band: 0.05

Step 3: clay input

Porosity (Φ) in
- host rock: 10 %
- deformation band: 3 %

Φ host vs. band: -70 %

Fig. 10: Porosity evolution of sample N-72-1. **(a)** Porosity after deformation band formation and before cementation. **(b)** Porosity after cementation and **(c)** after clay input. Note that pressure solution was not taken into account for complexity reason.

Figure 11

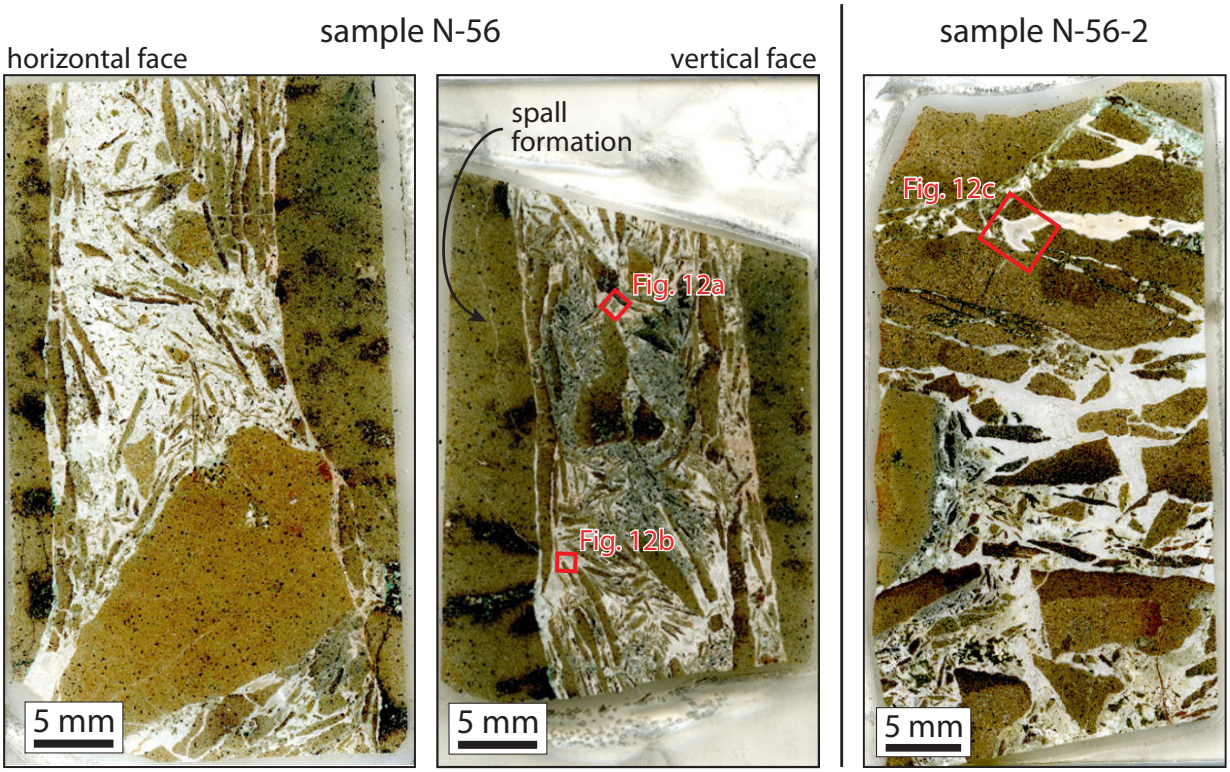

Fig. 11: Flatbed scans of thin sections of veins in the Etendeka basalt. Elongated fragments in the vein are interpreted as spalls (see text for explanation) and a spall may form in the upper left of the vertical face of sample N-56. Red squares mark location of close-ups (Fig. 12).

Figure 12

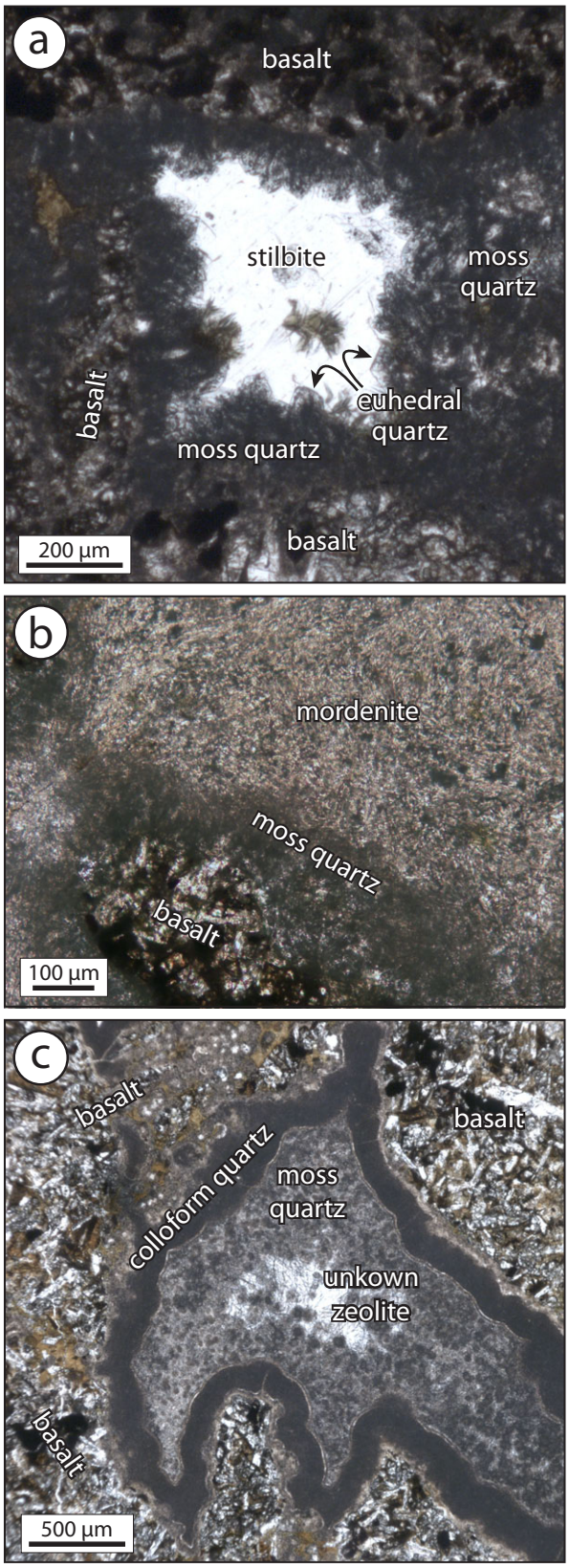

Fig. 12: Plane polarized images of vein components of sample N-56 **(a, b)** and N-56-2 **(c)**. **(a)** Moss quartz grows from basalt fragments and is capped by euhedral quartz when in contact with stilbite. **(b)** Euhedral quartz does not occur when moss quartz is in contact with mordenite. **(c)** Colloform quartz grows on basalt fragments and is followed by moss quartz, while an unidentified zeolite fills the cavity. Locations of images shown in **Fig. 11**. Raman spectra and SEM element maps of **(a)** are shown as supplementary figures.

Figure 13, revised

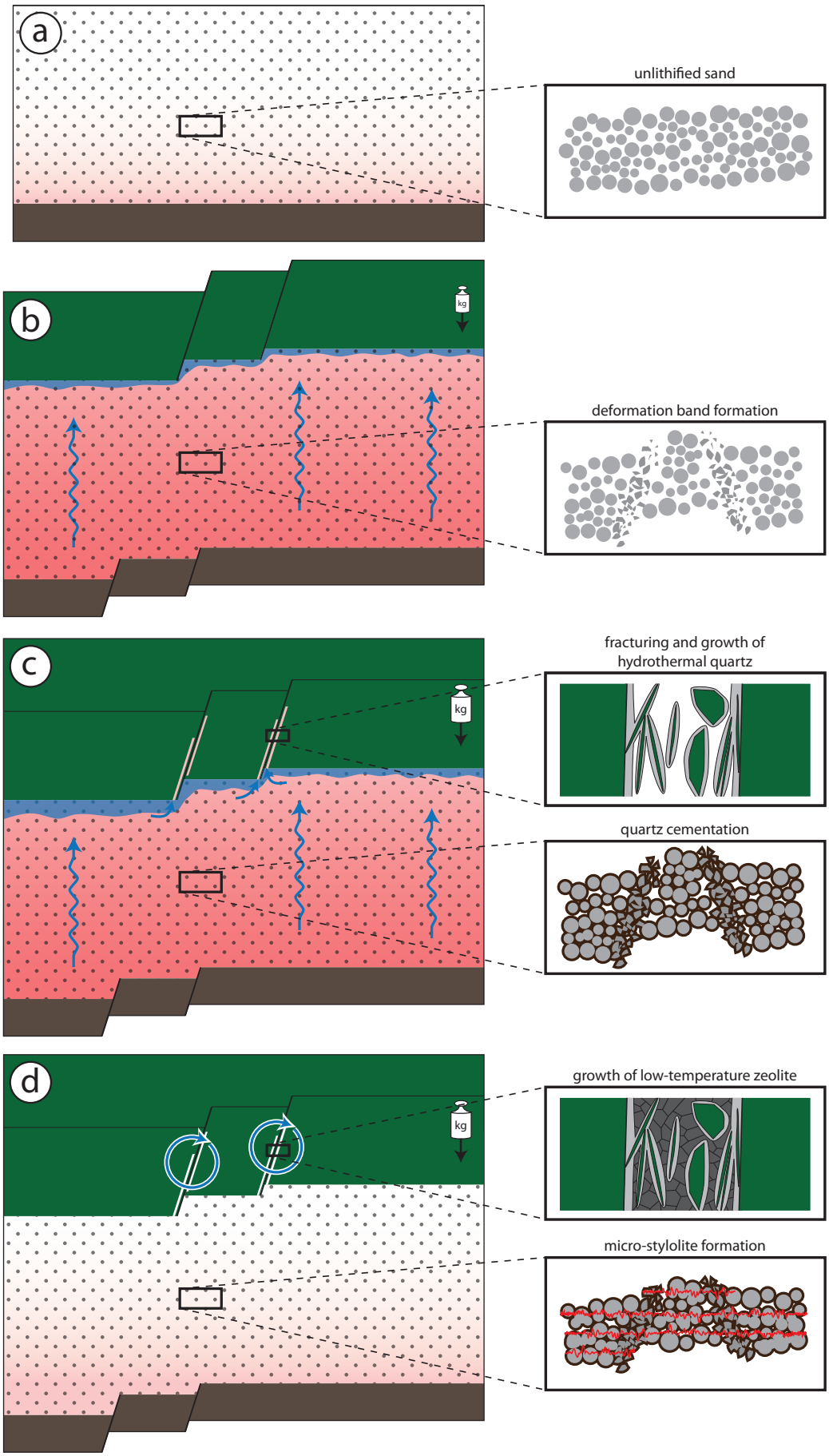

Fig. 13: Model of the evolution of deformation, fluid flow and crystal growth in the Twyfelfontein sandstone and Etendeka volcanic rocks. **(a)** Undisturbed groundwater flow through unlithified sandstone at a normal geothermal gradient. **(b)** Extrusion of volcanic rocks and formation of deformation bands due to syn-volcanic faulting. Volcanic activity leads to high geothermal gradient and increased fluid pressure underneath the volcanic rocks, which results in an escape of the fluid from the sandstone. **(c)** Increased fluid temperature leads to quartz cementation. Fracturing in volcanic rocks occur in response to fault movement or fluid pressure. The hot fluid penetrates into fractures causing spallation of wall rock and hydrothermal precipitation of quartz. **(d)** The geothermal gradient drops after the volcanic activity below a level where cementation is possible. Pressure solution deforms the sandstone and zeolite precipitates in veins due to inner-volcanic fluid circulation.

Table 1: Description of deformation band samples analyzed in this study.

Sample	Host Rock						Deformation Band					
	Colour	Mineralogy	Sorting	Grain shape	Grain Size	Clay content	Type	Thickness	Displacement	Offset	Dip direction	Dip angle
N-70	grey/pink	Quartz arenite	well sorted	sub-rounded	coarse	Kaolinite & Calcite	cataclastic	6 mm	/	no offset	087	84
N-72-1	reddish brown	Quartz arenite	well sorted	sub-rounded	coarse	Kaolinite	cataclastic	3 mm	1 cm	unknown	-	-
N-82	buff	Sublithic-arenite	poor	sub-angular	small pebbles	Fe-oxide	disaggrega-tion	3 mm	/	no offset	053	82
N-89	reddish brown	Sublithic-arenite	moderate	sub-angular	fine(75%) coarse(25%)	Kaolinite, Hematite	disaggrega-tion	1 mm	1 cm	normal	087	56
N-90	pale buff	Quartz arenite	very well sorted	sub-rounded	medium	Kaolinite	cataclastic	5 mm	/	no offset	085	83
N-92	reddish buff	Quartz arenite	moderate	sub-rounded	medium / coarse	Hematite	cataclastic	5 mm	1 cm	normal	053	60

Table 2: Porosity of deformation band samples derived from 2D image.

Sample	Outside band	Inside Band	Difference [%]
N-70	0.19	0.09	-53
N-72-1	0.10	0.03	-70
N-82	0.13	0.10	-23
N-89	0.09	0.10	+10
N-90	0.09	0.05	-44
N-92	0.08	0.03	-63